

EFFECT OF CHEMICAL INTERACTION ON BARENBLATT CRACK PROFILES IN BRITTLE SOLIDS

KAI-TAK WAN† and B. R. LAWN

Materials Science and Engineering Laboratory, National Institute of Standards and Technology,
Gaithersburg, MD 20899, U.S.A.

(Received 16 December 1991; in revised form 22 May 1992)

Abstract—A self-consistent solution for continuum-slit Barenblatt cracks with interactive chemistry is presented. Environmental species entering the crack mouth are limited in their transport along the ever-narrowing interface by molecular size restrictions. The ensuing cohesion zone behind the tip consists of three regions: an extended far region of weak solid–fluid–solid attraction; a small intermediate region of strong solid–fluid–solid repulsion; and an exclusionary near-tip intrinsic region of strong solid–solid attraction. To facilitate an analytical solution of the equations for the crack-opening displacements, the cohesion stresses are taken to be uniformly distributed within each of these zones. The magnitudes of these stresses are expressed in terms of the intersurface energies that define equilibrium crack states, for virgin and healed interfaces. Illustrative calculations of the crack profiles are given for the well-documented mica–water system. It is shown that the penetrating species cause a significant local bulge in the repulsion region, consistent with Thomson's picture of a molecular wedge.

Résumé—On présente une solution autocohérente des fissures de Barenblatt en fente continue avec chimie interactive. Les espèces environnantes entrant par l'ouverture de la fissure sont limitées dans leur transport le long de l'interface toujours étroite par des restrictions de taille des molécules. La zone de cohésion résultante derrière l'extrémité est formée de trois régions: une région assez étendue de faible attraction solide–fluide–solide; une petite région intermédiaire de forte répulsion solide–fluide–solide; une région intrinsèque d'exclusion, près de l'extrémité, de forte attraction solide–solide. Pour faciliter une solution analytique des équations donnant le déplacement d'ouverture de la fissure, les contraintes de cohésion sont prises uniformément réparties à l'intérieur de chacune de ces zones. La grandeur de ces contraintes est exprimée d'après les énergies interfaciales qui définissent les états d'équilibre des fissures, pour des interfaces vierge et perturbée. Des calculs de profils de fissures sont donnés pour le système bien connu mica–eau. On montre que les espèces pénétrantes provoquent un bombement local important dans la région de répulsion, en accord avec l'image de Thomson d'un coin moléculaire.

Zusammenfassung—Es wird eine selbstkonsistente Lösung für Bärenblatt-Kontinuums-Risse mit wechselwirkender Chemie vorgelegt. Die in die Rißmündung eindringenden Umgebungsspezies sind in ihrem Transport entlang der immer enger werdenden Grenzfläche wegen der Einschränkung durch die Molekülgröße behindert. Die folgende Kohäsionszone hinter der Spitze besteht aus drei Zonen: eine ausgedehnte Fernzone schwacher fest–flüssig–fester Wechselwirkung, einer kleinen Zwischenzone starker fest–flüssig–fester Abstoßung und einer exklusiven intrinsischen Zone in der Nähe der Spitze mit starker fest–fester Wechselwirkung. Zur Erleichterung der analytischen Lösung der Gleichungen für die Rißöffnungs-Verschiebung werden die Kohäsionsspannungen als gleichförmig in jeder dieser Zonen verteilt angenommen. Die Höhe dieser Spannungen wird anhand von Energien zwischen den Oberflächen, die den Gleichgewichtszustand des Risses definieren, für jungfräuliche und geheilte Grenzflächen ausgedrückt. Illustrierende Berechnungen der Rißprofile werden für das Wohlbekannte System Glimmer–Wasser durchgeführt. Es wird gezeigt, daß die eindringende Spezies eine beträchtliche Ausbeulung in der Abstoßungszone verursacht, welches verträglich ist mit Thomsons Vorstellung eines molekularen Keiles.

1. INTRODUCTION

In Irwin linear elastic fracture mechanics [1] the walls of continuum-slit cracks in ideally brittle solids are presumed to be traction-free. An inevitable consequence of this presumption is a pervasive singularity at the crack tip. The near-field crack-opening profile

is predicted to be parabolic, corresponding to an infinite crack-tip strain (or stress). Any such singularity is, of course, unphysical—intersurface cohesive bonds are intrinsically limited in the level of strain that they may sustain [2]. It was to remove the singularity that Barenblatt proposed his cohesion-zone theory [3], in which a distribution of cohesion intersurface stresses immediately *behind* the crack tip replaces a line of infinitesimally concentrated closure forces *at* the crack tip. The effect of the extended cohesion zone is to generate a crack-tip stress

†Doctoral Student, Department of Physics and Astronomy,
University of Maryland, College Park, MD 20742,
U.S.A.

intensity factor equal and opposite to that from externally applied loads—i.e. a “cancellation of K -fields”. Within the cohesion zone the crack walls close smoothly into a nonsingular cusp rather than into a singular Irwin parabola. In that the integral of the cohesive force-separation function defines a reversible surface energy, as it does in brittle ceramics [4], the Barenblatt model remains entirely consistent with the Griffith energy-balance concept of equilibrium fracture [2, 3].

Thus far, the Barenblatt model has been considered only for cracks in vacuum. Even there, attempts to determine actual near-tip crack profiles for specific brittle materials are few [5, 6]. Yet it is precisely in the near-tip region that the fundamental processes of crack propagation are decided. Given the interplanar stress p as a function of crack-plane coordinate x , $p(x)$, the Barenblatt profile can be formulated explicitly in terms of Green's function integrals. The difficulty is that p is not generally known *a priori* as a function of crack-plane coordinate x , but rather as a function of crack-opening displacement u , so we have $u(x) = f\{p[u(x)]\}$. A self-consistent approach to the Barenblatt problem thereby involves a nonlinear integral equation. Closed-form solutions of this nonlinear integral equation can be obtained only for the special case of an intersurface stress that is constant over the cohesive zone [2, 7].

For brittle cracks in an active environment, chemical interaction between the pristine surfaces and intrusive species adds a further degree of complexity. Detailed qualitative considerations of the atomic structure at crack interfaces in mica, sapphire and glass [8, 9] suggest that commonly deleterious environmental species like water do not generally have unlimited access to the crack tip—the size of the intruding molecules and the confinement of the closing walls are critical constraints in the solid–fluid–solid interaction within the cohesion (or adhesion) zone [8]. The invasive species, by virtue of their affinity with the crack surfaces, are sucked in to the crack-tip [10] region to a point where Born–Mayer repulsion with the solid atoms at the walls restricts any further progress, like a “molecular wedge” [9].

In this paper, we provide a simple quantitative analysis of the crack profile for a Barenblatt crack in an interactive environment. Our analysis retains the advantages of the continuum-slit description, by assuming that the intersurface stresses are distributed over a cohesion zone much larger than atomic dimensions. However, it also incorporates essential atomistic elements, by allowing for molecular size effects in the underlying force-separation function that governs equilibrium crack states, including *metastable* equilibrium states needed to account for crack healing [11]. To this end we distinguish the following regions of the cohesion zone [8]: (i) a far region of penetration by environmental species

some distance behind the crack tip where relatively weak attractive solid–fluid–solid interactions persist; (ii) an intermediate region closer to the tip where the adsorbing molecules begin to press against adjoining crack walls, producing a configurational solid–fluid–solid repulsion; (iii) a near-tip region where intervening molecules are excluded by the ever-confining walls, so that an attractive solid–solid interaction prevails. Explicit solutions of the nonlinear integral equations for the crack profile are then obtained in the approximation of *constant* intersurface stress within each of these regions. For illustration, equilibrium profiles are computed for the well-documented mica–water system [11, 12]. It is shown that whereas the overall effect of the environmental interaction is to reduce the crack opening, by virtue of a reduction in interface energy, the penetrating species cause a significant local bulge in the Born–Mayer repulsion region, consistent with the molecular-wedge picture. The model has strong implications concerning crack kinetics in brittle solids.

The same kind of chemically modified Barenblatt profiles are expected to apply to Hertzian-like contacts with adhesion [5, 13–15].

2. MODEL FOR BARENBLATT CRACK WITH CHEMICAL INTERACTION

In this section we first consider the fundamental stress- and energy-separation functions for an environmentally interactive solid–fluid–solid system, using the relatively well understood vacuum solid–solid system as a reference base. Then we determine specific crack-opening profiles using the Barenblatt formalism.

2.1. Fundamental energy- and stress-separation functions

To solve the general Barenblatt crack problem one needs information on the cohesive stresses $p(x)$ in Fig. 1. These cohesive stresses uniquely determine the equilibrium mechanical-energy-release rate J

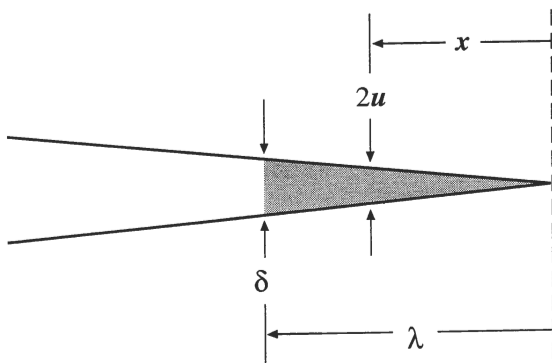


Fig. 1. Crack subjected to intersurface stresses over Barenblatt cohesion zone (shaded) of length λ and crack-opening displacement δ . Object of study is to determine the crack profile $u(x)$.

according to a Rice J -integral contour over the crack walls [16]

$$\begin{aligned}
 J &= 2 \int_0^\lambda p(x) (\partial u / \partial x) dx \\
 &= 2 \int_0^\delta p(u) du = 2\gamma
 \end{aligned}
 \tag{1}$$

where λ is the length of the cohesive zone along the crack-plane coordinate x , δ is the corresponding value of crack-opening displacement $2u$, and γ is an appropriate surface or interface energy. This simple relation foreshadows an underlying interchangeability between $p(x)$ and the more fundamental intersurface separation function $p(u)$ —the link is, of course, the $u(x)$ function that is the very object of this study.

Consider the separation of two planar solid walls separating in vacuum, Fig. 2(a), and in fluid, Fig. 3(a). For solid–solid interaction in *vacuum*, there is a single well-defined maximum in the stress-displacement function $p(u)$, and minimum in the corresponding energy-separation function $U(u)$. Our simplification here is to replace the smooth curves by the linearised approximations shown in Fig. 2(a), such that the cohesive stress is constant at p_0 over an interaction range δ_0 and the area under the $p(u)$ curve defines the bulk surface energy

$$2\gamma_B = p_0 \delta_0. \tag{2}$$

The equivalent construction for the solid–fluid–solid interaction in Fig. 3(a) is more complex. The work of separation of the *virgin* solid walls is

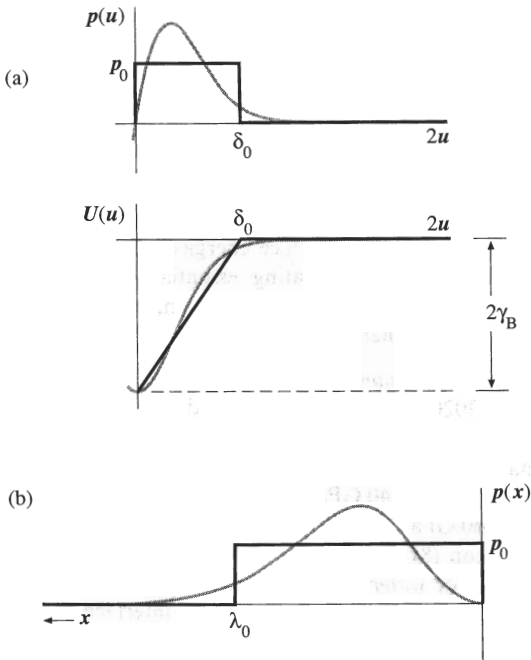


Fig. 2. Interaction diagrams for solid–solid system in *vacuum*. (a) Intersurface stress $p(u)$ and energy $U(u)$ as function of separation $2u$. (b) Corresponding stress $p(x)$ as function of distance x behind crack tip. Smooth functions are replaced by linearised approximations. Positive p designates attractive stresses.

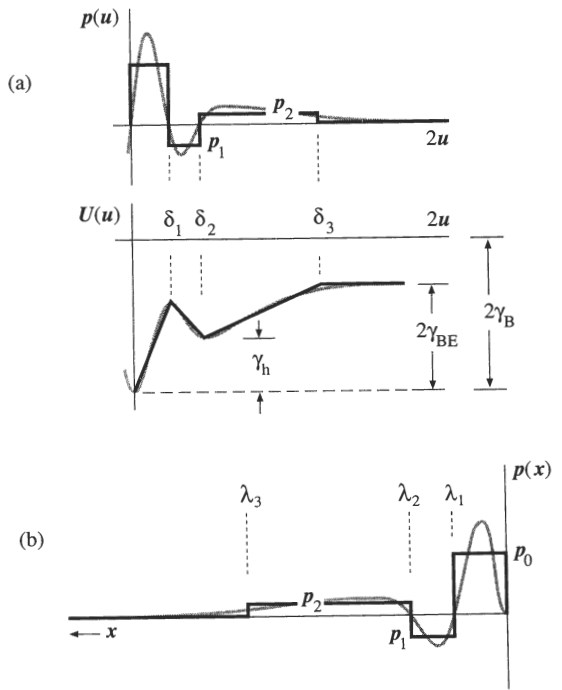


Fig. 3. As for Fig. 2, but for system in *interactive fluid*.

reduced by the environmental interaction to the interface energy $2\gamma_{BE}$. In general, the $U(u)$ function contains several subsidiary minima, allowing for metastable states [17]. These metastable states occur at separations approximately equal to integral numbers of fluid-molecule diameters, where the structure of the fluid is highly ordered [17, 18]—for our purpose, it is sufficient to consider just the first such subsidiary minimum. At small separations, the energy curve is identical to that in vacuum. Departure occurs beyond the first maximum, corresponding to penetration of the first layer of fluid molecules. On closing the solid walls the invasive layer may become trapped at the interface, increasing the energy level of the “closed interface” by a “fault energy” γ_h [11, 12]. This energy of formation of the occluded interface accounts for a further reduction work of separation to $2\gamma_{BE} - \gamma_h$ on repropagating cracks through *healed* interfaces. We note that the branch of negative slope on the $U(u)$ curve corresponds to a configurational repulsive stress $p(u)$. Once more replacing the smooth curves by linearised approximations, the areas under the $p(u)$ curve yield

$$2\gamma_{BE} = p_0 \delta_1 + p_1 (\delta_2 - \delta_1) + p_2 (\delta_3 - \delta_2) \tag{3a}$$

$$\gamma_h = p_0 \delta_1 + p_1 (\delta_2 - \delta_1) \tag{3b}$$

where p_0 , p_1 and p_2 are constant stresses, and δ_1 , δ_2 and δ_3 corresponding ranges, defining successive attractive, repulsive and attractive segments of the stress–separation curve.

We can use the above formulation to obtain useful relations for the stress and range parameters in terms of experimentally measurable quantities for our crack

profile calculations below. For *vacuum* separation, the range δ_0 is typically 1–3 times the spacing of atom layers bounding the cleavage plane. From equation (1)

$$p_0 = 2\gamma_B/\delta_0. \quad (4)$$

For separation in a *fluid*, the crack opening δ_2 at the subsidiary minimum is identified with the opening needed to accommodate one layer of the intruding molecules interstitially at the solid–solid interface. Simplistically, we suppose that the first energy maximum in Fig. 3(a) lies midway between the primary and subsidiary minima, $\delta_1 = \delta_2/2$. From equations (3) and (4) we obtain

$$p_1 = -2\gamma_B/\delta_0 + 2\gamma_h/\delta_2 \quad (5a)$$

$$p_2 = (2\gamma_{BE} - \gamma_h)/(\delta_3 - \delta_2). \quad (5b)$$

Generally, δ_2 is somewhat less than the true diameter of the fluid molecules (corresponding to a molecular compression <50%) [8]. The separation at which the interaction effectively cuts off may be long-ranged, $\delta_3 \gg \delta_2$ [17, 18].

2.2. Barenblatt crack profile relations

Now consider the crack-opening displacement profiles $u(x)$ for an equilibrium crack subjected to interplanar cohesion stresses. With our constant-stress approximations above it is straightforward to convert from fundamental intersurface $p(u)$ functions to crack-plane distribution functions $p(x)$ in the manner of Figs 2(b) and 3(b)—one has only to replace the delineating crack-opening displacements δ in equation (1) with corresponding cohesive-zone coordinates λ .

A general expression for a slit crack subjected to combined applied loads and cohesion-zone stresses follows from simple manipulations of Barenblatt's original analysis [2, 5, 19]

$$u(x) = (2/\pi E') \int_0^\lambda p[u(x')] [2(x/x')^{1/2} - \ln[(x'^{1/2} + x^{1/2})/(x'^{1/2} - x^{1/2})]] dx' \quad (6)$$

in the limit $\lambda \ll$ crack length; x is a field point and x' a source point; $E' = E/(1 - \nu^2)$ in plane strain, with E Young's modulus and ν Poisson's ratio. The first term in the square bracket at right represents the unstressed Irwin parabola, $u \propto x^{1/2}$; the second term represents the modifying effect of the intersurface stresses. It is readily shown that in the very-near crack-tip region of the cohesion zone, $x \ll \lambda$, the profile closes asymptotically into a cusp, $u \propto x^{3/2}$ [2, 5, 19].

First apply this formulation to the *vacuum* crack system depicted in Fig. 2(b). Cohesion stresses $p(x) = p_0$ act over $0 < x < \lambda_0$. Substituting into equation (6) and integrating gives

$$u(x) = (2p_0\lambda_0/\pi E') [2(x/\lambda_0)^{1/2} - (1 - x/\lambda_0) \ln[(\lambda_0^{1/2} + x^{1/2})/(\lambda_0^{1/2} - x^{1/2})]]. \quad (7)$$

At the edge of the cohesion zone, $2u = \delta_0$, $x = \lambda_0$, equation (7) may be combined with equation (2) to yield the simple relation

$$\lambda_0 = \pi E' \delta_0^2 / 16\gamma_B. \quad (8)$$

Now consider the crack in the *fluid environment*, Fig. 3(b). The cohesion stress zone subdivides into three regions: $p(x) = p_0$ over $0 < x < \lambda_1$; $p(x) = p_1$ over $\lambda_1 < x < \lambda_2$; $p(x) = p_2$ over $\lambda_2 < x < \lambda_3$. Substituting once more into equation (6) and integrating, we obtain

$$\begin{aligned} u(x) = (2/\pi E') \{ & (p_0 - p_1)\lambda_1 [2(x/\lambda_1)^{1/2} - (1 - x/\lambda_1) \\ & \times \ln[(\lambda_1^{1/2} + x^{1/2})/(\lambda_1^{1/2} - x^{1/2})]] \\ & + (p_1 - p_2)\lambda_2 [2(x/\lambda_2)^{1/2} - (1 - x/\lambda_2) \\ & \times \ln[(\lambda_2^{1/2} + x^{1/2})/(\lambda_2^{1/2} - x^{1/2})]] \\ & + p_2\lambda_3 [2(x/\lambda_3)^{1/2} - (1 - x/\lambda_3) \\ & \times \ln[(\lambda_3^{1/2} + x^{1/2})/(\lambda_3^{1/2} - x^{1/2})]] \}. \quad (9) \end{aligned}$$

The following boundary conditions may then be invoked: $2u(x = \lambda_1) = \delta_1$; $2u(x = \lambda_2) = \delta_2$; $2u(x = \lambda_3) = \delta_3$. This yields three implicit equations which may be solved simultaneously to obtain λ_1 , λ_2 and λ_3 .

3. CALCULATIONS FOR MICA-WATER CRACK SYSTEM

We illustrate the above analysis with computations on one of the best-studied brittle systems, muscovite mica in water. Mica is near-ideal because of its atomically smooth cleavage. This smoothness allows crack propagation to be studied with minimum complication, at both *virgin* and *healed* interfaces. Water is acknowledged as one of the most invasive environments in brittle cracks. Values of the necessary parameters in the crack-profile relations are obtainable from earlier considerations of the molecular structure of the mica–water interface [7] and experimental determinations of interface energies [11, 12, 20].

We begin by evaluating essential material parameters for the *virgin* mica system, using fracture data from earlier studies:

(i) For *vacuum*, the surface energy is taken as $2\gamma_B = 3020 \text{ mJ} \cdot \text{m}^{-2}$ [20]. The solid–solid intersurface stresses in mica are predominantly ionic, with estimated force–separation range $\delta_0 = 0.89 \text{ nm}$ [20]. This yields $p_0 = 3.40 \text{ GPa}$ from equation (4). With $E' = 60 \text{ GPa}$ [8], we obtain $\lambda_0 = 6.2 \text{ nm}$ from equation (8).

(ii) For *water*, measurement of equilibrium crack lengths reveal a greatly reduced interface energy, $2\gamma_{BE} = 276 \text{ mJ} \cdot \text{m}^{-2}$ [11, 12, 20]. Comparative measurements at healed interfaces provide an estimate of the “fault energy”, $\gamma_h = 124 \text{ mJ} \cdot \text{m}^{-2}$ [11, 12]. The wall–wall opening necessary to accommodate exactly one layer of water molecules of diameter 0.28 nm within 6-fold oxygen-coordinated interstitial sites at

Table 1. Barenblatt cohesion-zone parameters for mica in water, calculated using $p_0 = 3.40$ GPa, $p_1 = -1.84$ GPa, $\delta_0 = 0.89$ nm, $\delta_1 = 0.08$ nm, $\delta_2 = 0.16$ nm, for selected values of δ_3

δ_3/δ_2	p_2 (GPa)	λ_1 (nm)	λ_2 (nm)	λ_3 (nm)
5	0.238	0.45	0.99	22
10	0.106	0.44	0.95	83
20	0.050	0.44	0.93	320

the mica cleavage interface is $\delta_2 = 0.16$ nm [8]—the displacement $\delta_1 = \delta_2/2 = 0.08$ nm thereby corresponds to $\approx 30\%$ compression of the water molecules. Inserting this value of δ_2 into equation (5a) yields $p_1 = -1.84$ GPa, a substantial repulsive stress. Stresses p_2 evaluated from equation (5b) using a variety of ratios $\delta_3/\delta_2 = 5, 10, 20$ are seen in Table 1 to be relatively small. Table 1 includes corresponding values of the cohesion-zone dimensions λ_1, λ_2 and λ_3 evaluated numerically in accordance with the appropriate boundary conditions for equation (9).

Figure 4 shows the Barenblatt profile computed from equation (7), along with the reference Irwin parabola (limit of $\lambda_0 \rightarrow 0$), for mica in *vacuum*. (Note that the crack-opening axis is expanded relative to the crack-plane axis.) There is a strong pinching down of the crack into a cusp-like contour in the near field, $x \ll \lambda_0$, and asymptotic approach to the Irwin contour in the far field $x \gg \lambda_0$, as described by Barenblatt [3] and others [5]. The rather abrupt transition from the cusp to the open profile immediately outside the edge of the cohesion zone is undoubtedly exaggerated, owing to the artificial square-wave discontinuity in stress at $x = \lambda_0$ [Fig. 2(b)].

Analogous Barenblatt and reference Irwin crack profiles (limit of $\lambda_1, \lambda_2, \lambda_3 \rightarrow 0$) from equation (9) for mica in *water* are plotted in Fig. 5, for two of the three test values of δ_3/δ_2 : Fig. 5(a) focusses on the near field, $x < \lambda_3$, Fig. 5(b) on the far field, $x > \lambda_3$. A cusp is evident in the “protected zone” at $x < \lambda_1$, where the intrinsic solid–solid stress p_0 persists. In the intermediate zone $\lambda_1 < x < \lambda_2$, the action of the solid–fluid–solid overlap stress p_1 from the sucked-in molecules repels the walls, producing a pronounced

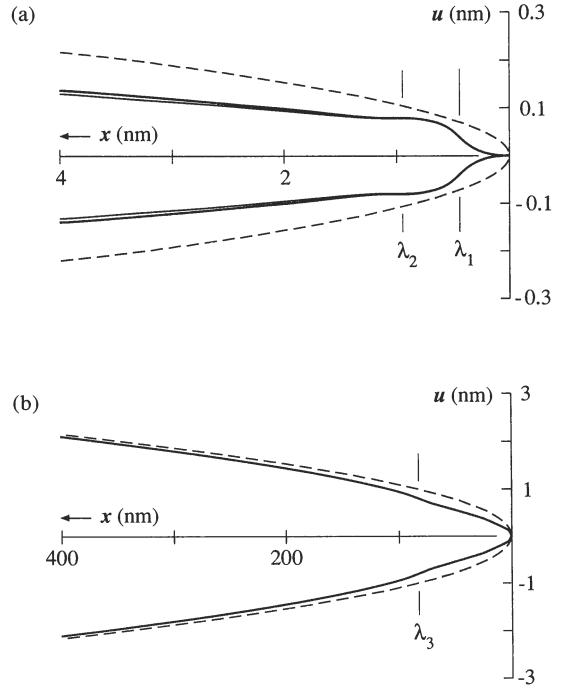


Fig. 5. Crack profile for virgin slit-crack, mica in water. Solid curves are Barenblatt profiles, equation (9). (a) Near field, for $\delta_3/\delta_2 = 5$ (outer profile) and 10 (inner profile); (b) far field, for $\delta_3/\delta_2 = 10$. Note expanded vertical scale. Dashed curve is reference Irwin parabola. Cusp-like closure is still evident at crack tip. However, outside immediate tip zone the crack walls open up under the repulsive action of invasive water molecules. In far field profile again approaches Irwin parabola.

bulge. The profile in this region is seen to be relatively insensitive to the choice of δ_3/δ_2 . Further from the tip, within $\lambda_2 < x < \lambda_3$, the longer range weak solid–fluid–solid attractive stress p_2 pulls the crack walls in again. Notwithstanding an artificial constriction at $x = \lambda_2$, due to the discontinuity in the stress function at that point [Fig. 3(b)], the crack opening is constrained at close to the diameter of water molecules over a distance of some tens of nm, dependent on δ_3/δ_2 . Ultimately, at $x \gg \lambda_3$, the profile tends again to the Irwin parabola.

It is informative to compare the equilibrium Barenblatt mica crack profiles for vacuum and water on the same diagram, as in Fig. 6. In the far field (not shown in Fig. 6) the crack opening in water is relatively narrow, because of the considerably lowered surface energy ($\gamma_{BE} \ll \gamma_B$). In the near field, however, the wedging action of the water molecules widens the crack beyond the reference vacuum profile. The crack opening close to the crack tip is clearly highly sensitive to the nature of the local cohesion stresses.

4. DISCUSSION

In this paper we have modified Barenblatt theory to compute the contours of brittle cracks in

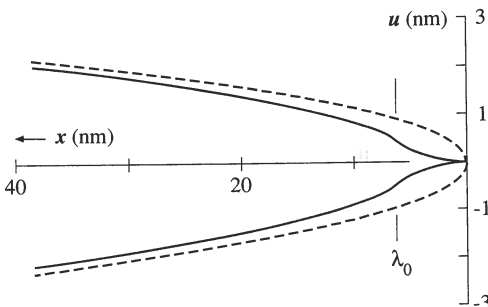


Fig. 4. Crack profile for virgin slit-crack, mica in vacuum. Note expanded vertical scale. Solid curve is Barenblatt profile, equation (7). Dashed curve is reference Irwin parabola. Observe cusp-like contour at crack tip at $x \leq \lambda_0$, asymptotic approach to Irwin contour outside cohesion zone at $x > \lambda_0$.

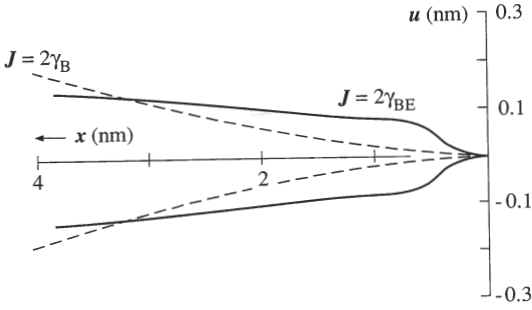


Fig. 6. Comparison of Barenblatt crack profiles for virgin mica, for equilibrium condition in equation (1): vacuum (Fig. 4), dashed curve; water (Fig. 5), solid curve (for $\delta_3/\delta_2 = 10$). Note expanded vertical scale.

chemically active fluid environments. Our model assumes that the fluid species at first manifest themselves as a weak wall-wall attraction, then a repulsion, as they penetrate down the ever-narrowing interface. The penetration is ultimately limited by molecular size constraints, leaving a small inaccessible cusp of strong solid-solid attraction immediately behind the crack tip. The approximation of constant intersurface stress within each of these successive attraction-repulsion-attraction regions allows simple solutions to an otherwise intractable nonlinear integral equation. Discontinuities in the stress distributions at the regional boundaries manifest themselves as unrealistic constrictions in the calculated contours, but these local perturbations do not detract from the principal physical conclusions. The formalism is expressed in terms of readily available quantities, appropriate interface energies measured from equilibrium crack configurations and molecular range parameters deduced from interface crystallography.

The calculations reinforce Thomson's "molecular wedge" conception of crack-tip chemistry [9]. Thus although water drastically reduces the interface energy of mica, and correspondingly reduces the far K -field at equilibrium applied load, the near-tip crack-opening displacement in Fig. 6 is significantly dilated by the molecular intrusion. This dilation may be attributed to a "configurational opening line force" averaged over the cohesion zone $0 < x < \lambda_3$ in Fig. 3(b)

$$\begin{aligned} \bar{q} &= -(\bar{p}_B - \bar{p}_{BE}) \\ &= -(2\gamma_B - 2\gamma_{BE})/\delta_3. \end{aligned} \quad (10)$$

Physically, the negative force \bar{q} is a manifestation of the real repulsion between $\lambda_1 < x < \lambda_2$ and the reduced attraction (adsorption, dielectric screening [11, 12, 20]) between $\lambda_2 < x < \lambda_3$. It may also be regarded as an equal but opposite line force exerted by the crack on the intruding molecular wedge, acting to expel the latter from the interface [9].

It is interesting to compare and contrast Thomson's calculations [9] of the mica-water crack-inter-

face structure with our own. Thomson used a lattice-crack model, with very specific assumptions concerning the discrete (dipolar) interactions of water molecules with (hard-sphere) constituent ions in the mica. His intermolecular functions were not expressly designed to match the relative interface energies of virgin and healed equilibrium cracks. The present quasi-continuum model incorporates these interface energies as critical parameters, without the need for any detailed knowledge of the underlying, discrete interactions. Despite this fundamental difference in approach, our quantitative estimates of the critical Barenblatt dimensions in the *secondary* (solid-fluid-solid) interaction zone agree in essence with Thomson. Thus in Fig. 5 there is a highly confined region of weak solid-fluid-solid attraction ($\lambda_3 > x > \lambda_2$) extending typically ≈ 100 nm along the x coordinate ($\delta_3/\delta_2 = 10$, Table 1), culminating in a leading edge of repulsion ($\lambda_2 > x > \lambda_1$) over ≈ 0.5 nm. On the other hand, whereas the continuum-slit constraint $u = 0$ at $x = 0$ artificially limits the inaccessible *primary* (solid-solid) interaction zone ahead of the molecular wedge ($\lambda_1 > x > 0$) to ≈ 0.5 nm in our model, Thomson's elastic lattice-plane Green's function more realistically accommodates (nonlinear) bond stretching over the extended crack plane ($\lambda_1 > x > -\infty$). Hence the present model inevitably underestimates the length of the inaccessible cusp [2].

Notwithstanding this last point of departure from physical reality, our simple linear elastic fracture mechanics does incorporate the essential scale of the environmental molecules within the structured mica interface. To consider the lattice discreteness more closely, we reproduce in Fig. 7 the water-modified Barenblatt crack for virgin mica from Fig. 5 using an appropriately scaled elastic-sphere construction [8], with cleavage-plane oxygen layers displaced outwardly from the bounding Barenblatt contours by one-half the equilibrium interlayer separation. Interlayer potassium ions maintain the oxygen layers at their zero-stress separation ahead of the crack tip. Water penetrates the interface to a configuration of $\approx 30\%$ molecular compression at available (6-fold oxygen-coordinated) interstices within the constraining mica surface structure (Section 3). Figure 7 is very different from the traditional picture of a continuum fluid with unrestricted access to the singular tip of a traction-free Irwin parabola [8].

The crack-interface configuration in Fig. 7 represents an equilibrium state. Increasing increments (or decrements) in the equilibrium K -field cause brittle cracks to extend (or contract) at monotonically increasing velocities [11, 21]. Traditionally, the kinetics have been attributed to the rates of concentrated reactions between the ingressing molecules and the terminal line of crack-tip bonds. It is evident from Fig. 7 that molecular diffusion along the constrained interface, particularly at the leading edge of the molecular wedge, is far more likely to be rate-controlling in mica. Thus far, such interfacial diffusional

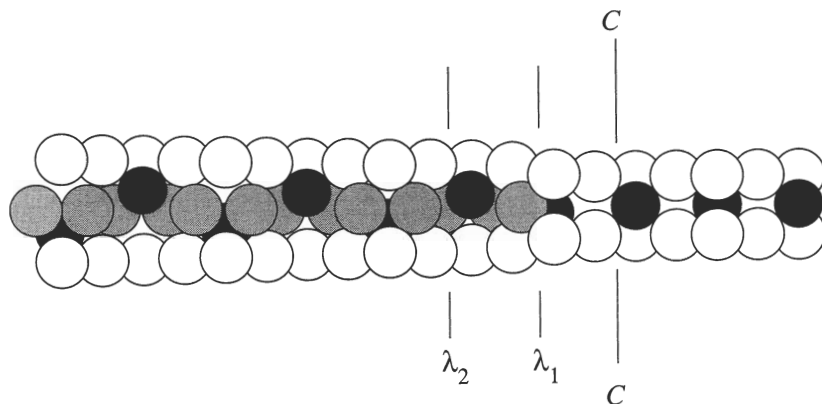


Fig. 7. Atomic representation of Barenblatt crack profile for mica-water system, redrawn from Fig. 5(a) but without expanded vertical scale. Atoms drawn to hard-sphere scale show bounding oxygen layers (open spheres) with intervening potassium ions (filled spheres) at the mica cleavage plane. Intrusive water molecules (shaded spheres) are allowed to penetrate to $x = \lambda_1$. CC designates crack tip, λ_1 and λ_2 cohesion zone dimensions. Structure after Ref. [8].

processes have received only phenomenological treatments in the literature [22].

It is also evident from Fig. 7 how a layer of invasive molecules is likely to be trapped at the interface in the event of crack retraction. The ensuing interface with occluded layer corresponds to the subsidiary minimum in Fig. 3(a). Repropagation through this metastable, "healed" interface requires less work to separate the walls relative to the virgin "ground state", by an amount equal to the fault energy γ_h [11, 12]. We emphasize that this energy term is explicitly incorporated into our crack profile analysis, through equation (5). If the exposed interface is rotated about a common normal prior to healing so that the recontacting surfaces are out of "lattice registry", γ_h is subject to increase [12, 20]. It is this last configuration that pertains most closely to adhesion states at contacting surfaces [13–15], as measured for instance in the Israelachvili surface forces apparatus [23].

In principle, the theoretical formulation in Section 2 applies to a broad range of ceramic-fluid crack interfaces [8]. At the mica cleavage plane, despite the fact that the packing of interlayer atoms is not too dense, the molecular wedge does not penetrate to the (nominal) crack tip. In sapphire the atoms at the fracture plane are much more closely packed, so the penetration is expected to be even less. In the opposite extreme of silicate glasses with "open" network structures the molecular wedge may penetrate with considerably less restriction—in this special case the traditional picture of a concentrated bond-rupture reaction may apply [24].

Acknowledgements—The authors are grateful to W. C. Carter, E. R. Fuller, R. G. Horn and R. M. Thomson for discussions. Funding was provided by the U.S. Office of Naval Research.

REFERENCES

1. G. R. Irwin, in *Handbuch der Physik*, Vol. 6, p. 551. Springer, Berlin (1958).
2. B. R. Lawn, *Fracture of Brittle Solids*, 2nd edn, Chap. 3. Cambridge Univ. Press, Cambridge (1992).
3. G. I. Barenblatt, *Adv. appl. Mech.* **89**, 55 (1962).
4. B. R. Lawn, B. J. Hockey and S. M. Wiederhorn, *J. Mater. Sci.* **15**, 1207 (1980).
5. J. A. Greenwood and K. L. Johnson, *Phil. Mag. A* **43**, 697 (1981).
6. D. Y. C. Chan, B. D. Hughes and L. R. White, *J. Colloid Interface Sci.* **115**, 240 (1987).
7. D. S. Dugdale, *J. Mech. Phys. Solids* **8**, 100 (1960).
8. B. R. Lawn, D. H. Roach and R. M. Thomson, *J. Mater. Sci.* **22**, 4036 (1987).
9. R. Thomson, *J. Mater. Res.* **5**, 524 (1990).
10. B. R. Lawn, *J. Mater. Sci.* **12**, 1950 (1977).
11. K.-T. Wan, N. Aimard, S. Lathabai, R. G. Horn and B. R. Lawn, *J. Mater. Res.* **5**, 172 (1990).
12. K.-T. Wan and B. R. Lawn, *Acta metall. mater.* **38**, 2073 (1990).
13. K. L. Johnson, K. Kendall and A. D. Roberts, *Proc. R. Soc. Lond. A* **324**, 301 (1971).
14. B. V. Derjaguin, V. M. Muller and Yu. P. Toporov, *J. Colloid Interface Sci.* **53**, 314 (1975).
15. D. Maugis and M. Barquins, *J. phys. D: Appl. Phys.* **11**, 1989 (1978).
16. J. R. Rice, *J. appl. Mech.* **35**, 379 (1968).
17. R. G. Horn and J. N. Israelachvili, *J. chem. Phys.* **75**, 1400 (1981).
18. J. N. Israelachvili, *Intermolecular and Surface Forces*. Academic Press, New York (1985).
19. R. A. Schapery, *Int. J. Fract.* **11**, 369 (1975).
20. K.-T. Wan, D. T. Smith and B. R. Lawn, *J. Am. Ceram. Soc.* **75**, 667 (1992).
21. K.-T. Wan, S. Lathabai and B. R. Lawn, *J. Eur. Ceram. Soc.* **6**, 259 (1990).
22. B. R. Lawn and S. Lathabai, *Mater. Forum* **11**, 313 (1988).
23. R. G. Horn, J. N. Israelachvili and F. Pribac, *J. Colloid Interface Sci.* **115**, 480 (1987).
24. T. A. Michalske and S. W. Freiman, *Nature* **295**, 511 (1981).